Proceedings of the
Annual Stability Conference
Structural Stability Research Council
San Antonio, Texas, March 19-22, 2024

On the buckling and post-buckling behavior of thin-walled pre-twisted columns

Nuno Peres[1], Rodrigo Gonçalves[2]

Abstract
A beam finite element for pre-twisted beams is presented and employed to assess the linear, buckling and post-buckling behavior of uniformly compressed members (columns) with thin-walled rectangular section. The element follows the so-called "geometrically exact" concept and can be viewed as an extension/specialization, to the pre-twisted case, of that previously developed by the authors (Peres et al. 2021). Torsion-related warping and arbitrary mid-line warping/extension effects are included. As shown in the examples presented in the paper, the element is capable of capturing the twist-extension coupling that occurs even in the linear case. In fact, the element provides very accurate linear, buckling and post-buckling solutions for pre-twisted columns.

1. Introduction

Pre-twisting a column has a beneficial stiffening effect due to the change of the weak axis direction along the length of the member. Consequently, pure minor-axis buckling is no longer possible, leading to a higher critical buckling load. However, conversely, pure major-axis buckling is also impossible. A detailed account of the research in the relatively vast field of pre-twisted rods, including the buckling case (among others), can be found in Rosen (1991). For the buckling case, the most relevant papers concerning beam-type formulations can be divided according to whether the so-called "helical fiber assumption" — the longitudinal fibers form helices — is adopted (Zickel 1956) or not (Ziegler 1951, Frisch-Fay 1973, Tabarrok et al. 1990, Steinman et al. 1991). However, none of these formulations allow cross-section warping and transverse extension. In fact, thin-walled pre-twisted members exhibit peculiar structural features which are challenging to model using beam elements, making it invariably necessary to resort to computationally expensive shell finite element models.

This paper extends/specializes the beam finite element proposed in Peres et al. (2021) to the pre-twisted case and uses it to investigate the linear, buckling and post-buckling behavior of pre-twisted columns. The element is capable of capturing all the relevant effects in pre-twisted members, namely the twist-extension coupling that occurs even in the geometrically linear case, and allows arbitrary cross-section warping and mid-line expansion/contraction (transverse

[1] Assistant Professor, CERIS and Universidade Lusófona, Portugal <nuno.peres@ulusofona.pt>
[2] Full Professor, CERIS and Universidade Nova de Lisboa, Portugal <rodrigo.goncalves@fct.unl.pt>

extension), through additional cross-section DOFs. Since the element is geometrically exact — meaning that the underlying formulation is independent of the magnitude of the displacements and rotations involved (Reissner 1972, 1973; Simo 1985) —, it allows calculating very accurate linear, buckling and post-buckling solutions up to large displacements and finite rotations. The accuracy of the proposed element is demonstrated through comparison with refined shell finite element models, even in case of high pre-twist.

2. A beam finite element for pre-twisted thin-walled beams

The approach followed in this paper constitutes an extension/specialization of that proposed in Peres et al. (2021) to the pre-twisted case. Fig. 1 shows the initial and current configuration of a pre-twisted beam with narrow rectangular section, where t is the thickness, assumed inextensible. The initial configuration is mapped through

$$\boldsymbol{x}_0 = X_3\boldsymbol{E}_3 + \boldsymbol{\Lambda}_0 X_2\boldsymbol{E}_2 + X_1\boldsymbol{n}_0, \tag{1}$$

where the cross-section mid-line rotation matrix $\boldsymbol{\Lambda}_0$ is given by

$$\boldsymbol{\Lambda}_0 = \begin{bmatrix} \cos\theta_0 & -\sin\theta_0 & 0 \\ \sin\theta_0 & \cos\theta_0 & 0 \\ 0 & 0 & 1 \end{bmatrix}, \tag{2}$$

which depends on the pre-twist angle $\theta_0 = \theta_0(X_3)$, and $\boldsymbol{n}_0$ is the through-thickness director, assumed perpendicular to the mid-surface, hence the cross-section has an initial torsion-related warping as shown in the figure.

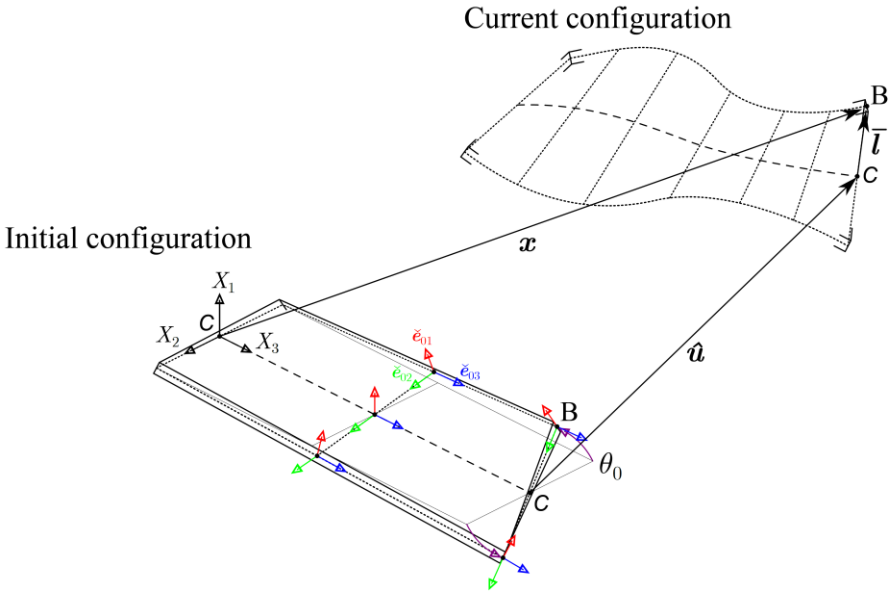

Figure 1: Initial and current configurations of the pre-twisted beam

The current configuration is defined using

$$\boldsymbol{x} = X_3\boldsymbol{E}_3 + \hat{\boldsymbol{u}} + \hat{\boldsymbol{\Lambda}}\boldsymbol{\Lambda}_0\bar{\boldsymbol{l}} + X_1\boldsymbol{n}, \tag{3}$$

thus $\widehat{\boldsymbol{u}} = \widehat{\boldsymbol{u}}(X_3)$ is the displacement of the centroid *C*. The cross-section mid-line rotates according to the rotation tensor $\widehat{\boldsymbol{\Lambda}} = \widehat{\boldsymbol{\Lambda}}(X_3)$, which is parametrized with the rotation vector $\widehat{\boldsymbol{\theta}}$ (see e.g. Goldstein, 1980), and is described in the co-rotational frame $\widehat{\boldsymbol{\Lambda}}\boldsymbol{\Lambda}_0\boldsymbol{E}_i$ through

$$\bar{\boldsymbol{l}} = X_2\boldsymbol{E}_2 + \sum_{i=1}^{D}\left(\bar{\chi}_2^{(i)}\boldsymbol{E}_2 + \bar{\chi}_3^{(i)}\boldsymbol{E}_3\right)\hat{p}^{(i)}, \tag{4}$$

using $i = 1, \ldots, D$ prescribed deformation modes with warping ($\bar{\chi}_3^{(i)}$) and transverse extension ($\bar{\chi}_2^{(i)}$) components, whose amplitudes along the axis are given by $\hat{p}_j^{(i)} = \hat{p}_j^{(i)}(X_3)$, and $\boldsymbol{n}$ is the through-thickness director.

Proceeding as explained in Gonçalves et al. (2010) and Peres et al. (2021), assuming small bending strains, the Green-Lagrange strains can be subdivided into membrane and bending components. The membrane components are given by

$$\boldsymbol{E}^M = \frac{1}{2}\breve{\boldsymbol{\Lambda}}_0^{\mathrm{T}}\boldsymbol{F}_0^{-\mathrm{T}}\boldsymbol{A}\boldsymbol{F}_0^{-1}\breve{\boldsymbol{\Lambda}}_0, \tag{5}$$

$$\breve{\boldsymbol{\Lambda}}_0 = \breve{\boldsymbol{e}}_{01}\otimes\boldsymbol{E}_1 + \breve{\boldsymbol{e}}_{02}\otimes\boldsymbol{E}_2 + \breve{\boldsymbol{e}}_{03}\otimes\boldsymbol{E}_3, \tag{6}$$

$$\boldsymbol{F}_0 = \frac{\mathrm{d}\boldsymbol{x}_0}{\mathrm{d}\boldsymbol{X}}, \tag{7}$$

$$\boldsymbol{A} = (\boldsymbol{g}_2\cdot\boldsymbol{g}_2)\boldsymbol{E}_2\otimes\boldsymbol{E}_2 + (\boldsymbol{g}_3\cdot\boldsymbol{g}_3)\boldsymbol{E}_3\otimes\boldsymbol{E}_3 + (\boldsymbol{g}_2\cdot\boldsymbol{g}_3)(\boldsymbol{E}_2\otimes\boldsymbol{E}_3 + \boldsymbol{E}_3\otimes\boldsymbol{E}_2), \tag{8}$$

$$\boldsymbol{g}_i = \widehat{\boldsymbol{\Lambda}}^{\mathrm{T}}\boldsymbol{\Lambda}_0^{\mathrm{T}}\boldsymbol{x}_{,i}, \tag{9}$$

where $\boldsymbol{f}_{,i} = \mathrm{d}\boldsymbol{f}/\mathrm{d}X_i$. Note that the strains are back-rotated to the "local" frame in each mid-surface point, $\breve{\boldsymbol{e}}_{0i}$ (see Fig. 1) to ensure a correct mid-surface description, using the rotation tensor $\breve{\boldsymbol{\Lambda}}_0$, which can be calculated from the directors

$$\breve{\boldsymbol{e}}_{03} = \frac{\boldsymbol{F}_0\boldsymbol{E}_3}{||\boldsymbol{F}_0\boldsymbol{E}_3||}, \tag{10}$$

$$\breve{\boldsymbol{e}}_{01} = \boldsymbol{n}_0 = \frac{(\boldsymbol{F}_0\boldsymbol{E}_2)\times(\boldsymbol{F}_0\boldsymbol{E}_3)}{||(\boldsymbol{F}_0\boldsymbol{E}_2)\times(\boldsymbol{F}_0\boldsymbol{E}_3)||}, \tag{11}$$

$$\breve{\boldsymbol{e}}_{02} = \breve{\boldsymbol{e}}_{03}\times\breve{\boldsymbol{e}}_{01}. \tag{12}$$

It can be demonstrated that this approach effectively leads to only three non-null membrane strain components: E_{22}^M, E_{33}^M and E_{23}^M.

The bending strains are given by

$$\boldsymbol{E}^B = E_{33}^B\boldsymbol{E}_3\otimes\boldsymbol{E}_3 + E_{23}^B(\boldsymbol{E}_2\otimes\boldsymbol{E}_3 + \boldsymbol{E}_3\otimes\boldsymbol{E}_2) + E_{13}^B(\boldsymbol{E}_1\otimes\boldsymbol{E}_3 + \boldsymbol{E}_3\otimes\boldsymbol{E}_1), \tag{13}$$

$$E_{33}^B = -X_1\left(\hat{\kappa}_2 - \hat{p}_{t,3}X_2\right), \tag{14}$$

$$E_{23}^B = \frac{X_1}{2}(\hat{\kappa}_3 + \hat{p}_t), \tag{15}$$

$$E_{13}^B = \frac{1}{2}(-\hat{\kappa}_3 + \hat{p}_t)X_2 + \frac{1}{2}\hat{\Gamma}_1, \tag{16}$$

where $\hat{\kappa}_2$ is the bending curvature, $\hat{\kappa}_3$ is the torsion curvature, $\hat{\Gamma}_1$ is the through-thickness shearing (a novelty of the proposed formulation) and $\hat{p}_t = \hat{p}_t(X_3)$ is the amplitude of the torsion-related warping. The independent kinematic parameters are grouped as follows

$$\widehat{\boldsymbol{\phi}} = \begin{bmatrix} \widehat{\boldsymbol{u}} \\ \widehat{\boldsymbol{\theta}} \\ \hat{p}^{(1)} \\ \vdots \\ \hat{p}^{(D)} \\ \hat{p}_t \end{bmatrix}. \tag{17}$$

A St. Venant-Kirchhoff material law is adopted, with the membrane and bending second Piola-Kirchhoff stresses related to the corresponding strains through

$$\widehat{\boldsymbol{S}}^M = \boldsymbol{C}^M \widehat{\boldsymbol{E}}^M,\ \widehat{\boldsymbol{S}}^M = \begin{bmatrix} \hat{S}^M_{22} \\ \hat{S}^M_{33} \\ \hat{S}^M_{23} \end{bmatrix}, \widehat{\boldsymbol{E}}^M = \begin{bmatrix} \hat{E}^M_{22} \\ \hat{E}^M_{33} \\ 2\hat{E}^M_{23} \end{bmatrix},\ \boldsymbol{C}^M = \begin{bmatrix} \frac{E}{1-\nu^2} & \frac{\nu E}{1-\nu^2} & 0 \\ \frac{\nu E}{1-\nu^2} & \frac{E}{1-\nu^2} & 0 \\ 0 & 0 & G \end{bmatrix} \text{ or } \boldsymbol{C}^M = \begin{bmatrix} 0 & 0 & 0 \\ 0 & E & 0 \\ 0 & 0 & G \end{bmatrix}, \tag{18}$$

$$\widehat{\boldsymbol{S}}^B = \boldsymbol{C}^B \widehat{\boldsymbol{E}}^B,\ \widehat{\boldsymbol{S}}^B = \begin{bmatrix} \hat{S}^B_{33} \\ \hat{S}^B_{23} \\ \hat{S}^M_{13} \end{bmatrix},\ \widehat{\boldsymbol{E}}^B = \begin{bmatrix} \hat{E}^M_{33} \\ 2\hat{E}^M_{23} \\ 2\hat{E}^M_{13} \end{bmatrix},\ \boldsymbol{C}^B = \begin{bmatrix} E & 0 & 0 \\ 0 & G & 0 \\ 0 & 0 & G \end{bmatrix}, \tag{19}$$

where E is Young's modulus and G is the shear modulus, and the second version of $\boldsymbol{C}^M$ applies if the cross-section mid-line is not allowed to undergo transverse extension ($\bar{\chi}_2^{(i)} = 0$).

The virtual work statement reads

$$\delta W = -\int_V \left(\delta(\widehat{\boldsymbol{E}}^M)^{\mathrm{T}}\, \widehat{\boldsymbol{S}}^M + \delta(\widehat{\boldsymbol{E}}^B)^{\mathrm{T}}\, \widehat{\boldsymbol{S}}^B\right) J_0 \mathrm{d}V + \delta\boldsymbol{x} \cdot \boldsymbol{Q} = 0, \tag{20}$$

where V is the beam volume without pre-twist, hence the change in volume $J_0 = \det(\boldsymbol{F}_0)$ must be introduced, and the external work is herein restricted to concentrated forces $\boldsymbol{Q}$. As shown in Peres et al. (2021), it is possible to write the equilibrium equations and their linearization in terms of the parameters in $\widehat{\boldsymbol{\phi}}$, using the auxiliary matrices introduced in Gonçalves et al. (2010) and Ritto-Corrêa & Camotim (2002).

The beam finite element approximates the parameters in $\widehat{\boldsymbol{\phi}}$ using Hermite cubic polynomials, hence a 2-node element with $4(7 + D)$ DOFs is obtained, where D is the number of deformation modes besides torsion-related warping. Legendre polynomials are used to define $\bar{\chi}_2^{(i)}$ and $\bar{\chi}_3^{(i)}$, excluding the linear dependence with respect to rigid-body motions. The equilibrium paths are calculated with a standard incremental/iterative scheme with load and displacement control, using MATLAB (2018). The integrations rely on 3 Gauss points along the length (reduced integration) and a sufficiently high number of points along the cross-section mid-line, to ensure capturing accurately the pre-twist effects. The bending terms are integrated analytically.

3 Numerical examples

All results presented next concern pre-twisted cantilever columns with constant pitch (θ_0 is linear in X_3). The free end load is uniformly distributed. The geometry and material parameters are as follows: 300 mm width, 10 mm thickness, 3 m length, $E = 210$ GPa and $\nu = 0.3$. A preliminary mesh convergence study for the proposed beam element was carried out, showing that 50 equal length elements suffice in all cases presented next. However, it should be noted that less elements are generally required. For comparison purposes, results obtained with refined shell finite element models are provided, using the MITC-4 element and ADINA (Bathe 2022).

3.1 Linear analysis

First, linear analyses are performed to assess the ability of the proposed beam finite element to capture torsion-extension coupling. Cantilever columns subjected to a 1 kN axial force, with varying pre-twist, are analyzed and the results are presented in Fig. 2 and 3. The graphs b)-d) plot the end section rotation and longitudinal displacements of points A and C, as a function of the total pre-twist, obtained with the reference solution (shell, ADINA) and the beam model with or without warping (W) and transverse extension (TE) deformation modes. Furthermore, the influence of back-rotating the membrane strains using either $\breve{\mathbf{\Lambda}}_0$ or simply $\mathbf{\Lambda}_0$ is also investigated. When the modes are included, Legendre polynomials up to degree 8 for W and 7 for TE are considered.

These results make it possible to draw the following conclusions:

(i) Back-rotating the strains using $\mathbf{\Lambda}_0$ can be considered acceptable for angles up to 400º, but not beyond this value, as the errors start to increase.

(ii) It is indispensable to use W and TE modes to capture accurately the longitudinal displacement of point A and the end rotation, while the longitudinal displacement of point C does not require the inclusion of deformation modes. Nevertheless, it should be remarked that the proposed element leads to excellent results even for very high pre-twist.

(iii) Graph b) shows the well-known extension-torsion coupling effect in pre-twisted beams: the beam twists under compression. However, this effect first increases with the pre-twist, up to approximately 90º, and then decreases (being always positive).

(iv) Graphs c) and d) make it possible to conclude that the longitudinal displacement of points A and C always increases with the pre-twist, although the relation is non-linear.

(v) The deformed configurations in Fig. 3 clearly show that the proposed element with W+TE modes can reproduce very accurately the shell model solutions, which exhibit severe end-section warping. Besides the untwisting effect, it is observed that the cross-sections expand transversally; however, the latter effect is partially due to the use of linearized rotations in the representation of the configurations.

3.2 Buckling analysis

The bifurcation loads and buckling modes are calculated on the basis of the linear stability analysis concept, thus the effect of pre-buckling deflections is not considered. The pre-buckling stresses are calculated by performing a linear analysis and then the "initial stress" tangent stiffness matrix is evaluated. The bifurcation loads and buckling modes are obtained from the condition of singularity of the tangent stiffness matrix.

Table 1 displays the first two bifurcation loads obtained with the shell models (ADINA), the solution of Tabarrok et al. (1990) and the proposed beam finite element. The errors are measured

with respect to the shell model solutions, which show that, as expected, the critical bifurcation load increases with the pre-twist, while the second one decreases (for straight columns the solutions are 1.439 and 12.95 kN and correspond to minor axis buckling only). The solution of Tabarrok et al.

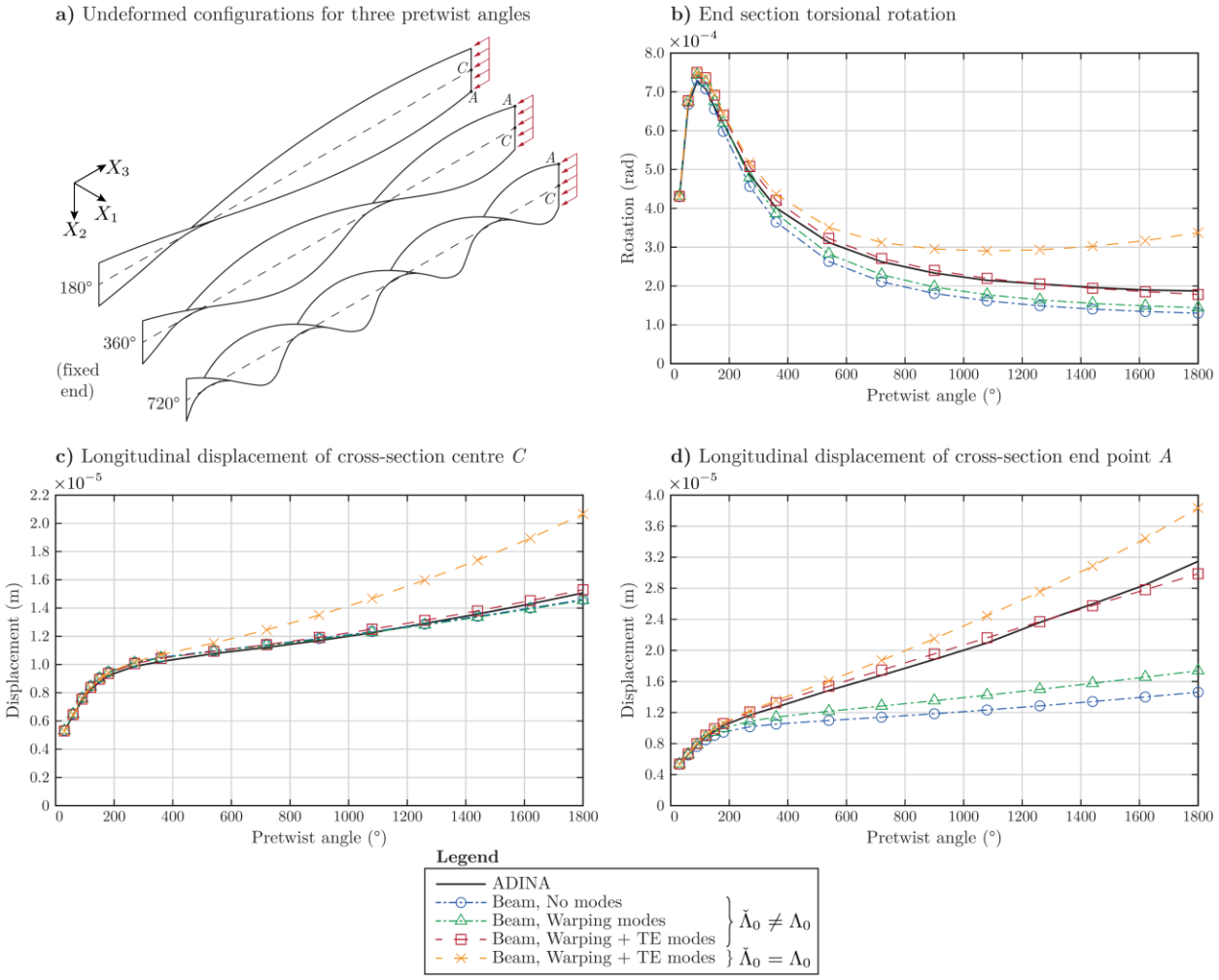

Figure 2: Linear analysis of pre-twisted cantilever columns

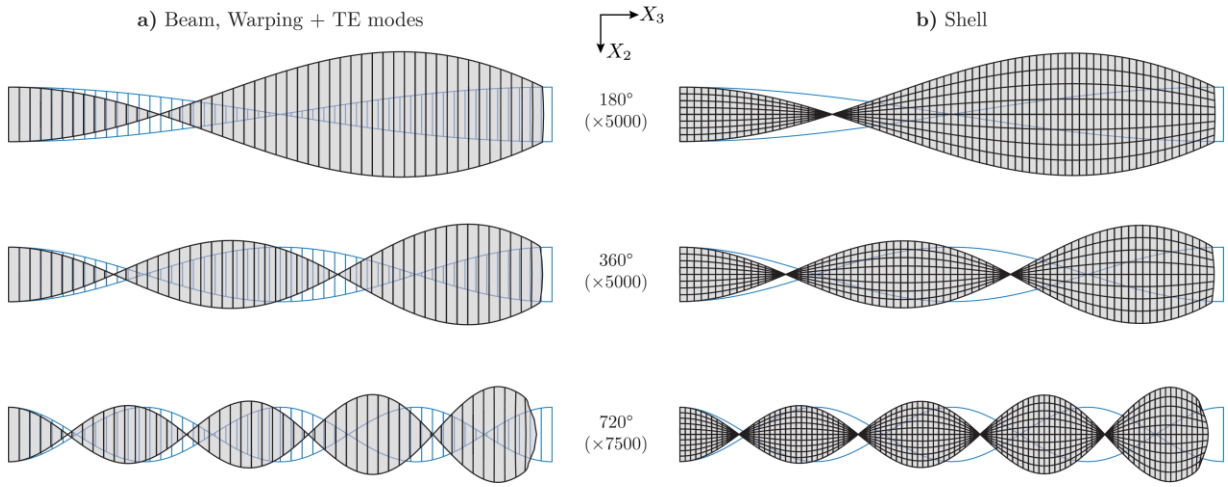

Figure 3: Linear analysis of pre-twisted cantilever columns: deformed configurations

(1990) leads a significant error, most probably because it does not account for the helical nature of the longitudinal fibers and the cross-sections are not pre-warped (as in the shell model and the proposed beam finite element used in this paper). On the other hand, the proposed element leads to very accurate solutions. It is worth remarking that, even though the W and TE modes are necessary to obtain accurate pre-buckling solutions, their effect on the bifurcation loads is not significant and is not shown in the table.

Table 1: First two bifurcation loads (kN) for pre-twisted columns

Pre-twist	Mode	ADINA	Tabarrok et al. (1990)		Beam, 50 FE	
180º	1	1.9619	2.5728	31.14%	1.9677	0.30%
	2	4.2270	3.1883	-24.57%	4.2148	-0.29%
360º	1	2.4023	2.7240	13.39%	2.4600	2.40%
	2	3.3207	3.0292	-8.78%	3.4119	2.75%

Finally, the buckling modes obtained with the reference solution and the proposed element can be compared in Figs. 4 and 5. Clearly, an excellent match is observed. It is worth noting that the beam axis assumes a space curve configuration, rather than a plane one, as in the prismatic case.

3.3 Post-buckling analysis

Finally, the load-displacement path is traced for the 180º pre-twist case, seeding a small critical mode shape (mode 1 in Fig. 4) initial imperfection in the beam and shell models, scaled so that the displacement of the free end along X_2 equals 1 cm. The reference loading corresponds to a 1 kN load hence the load parameter λ indicates the load in kN. The results are show in Figs. 6 and 7.

The load-displacement graph show that post-buckling is stable and a good agreement can be observed between both models, even if the differences increase above as the load increases beyond the critical load (1.96 kN according to the shell model, 1.97 kN from the beam model). The deformed configurations further confirm these findings, since there are small differences for $\lambda \geq$ 2.0 kN.

4 Conclusion

This paper presented a geometrically exact beam finite element for pre-twisted thin-walled rectangular section members, which was used to investigate the structural behavior of pre-twisted columns. The proposed element is capable of capturing all the relevant effects in pre-twisted members, namely twist-extension coupling (triggered even in the linear case), primary (membrane) and secondary (namely torsion-related) warping, and mid-line transverse extension. The examples presented in the paper show that the element is capable of providing linear, buckling and post-buckling solutions that match very accurately those obtained with refined shell finite element models, even for high pre-twist.

One final word to mention that work is currently under way to extend the element to cross-sections with multiple walls.

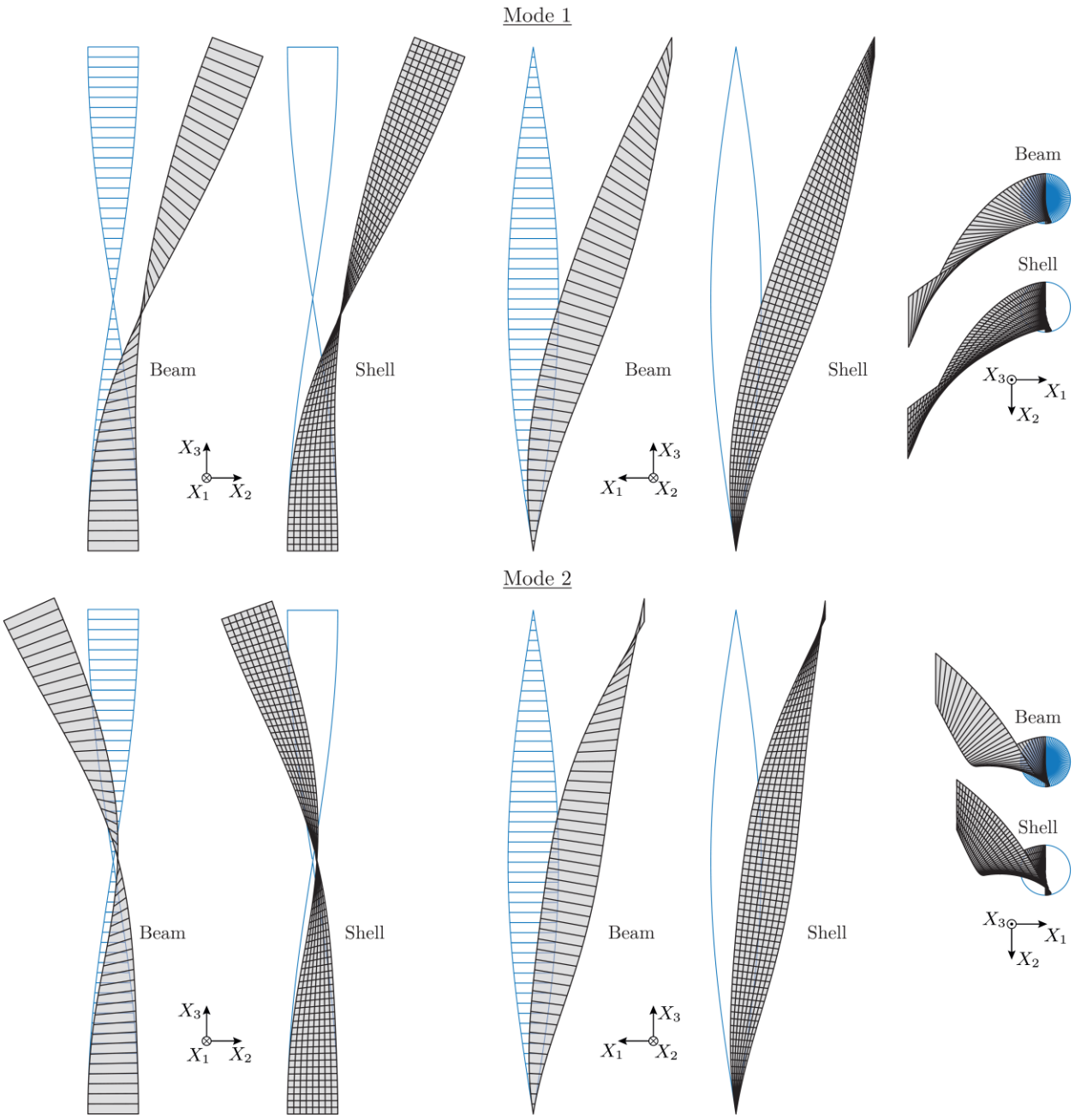

Figure 4: First two buckling modes for a 180º pre-twist

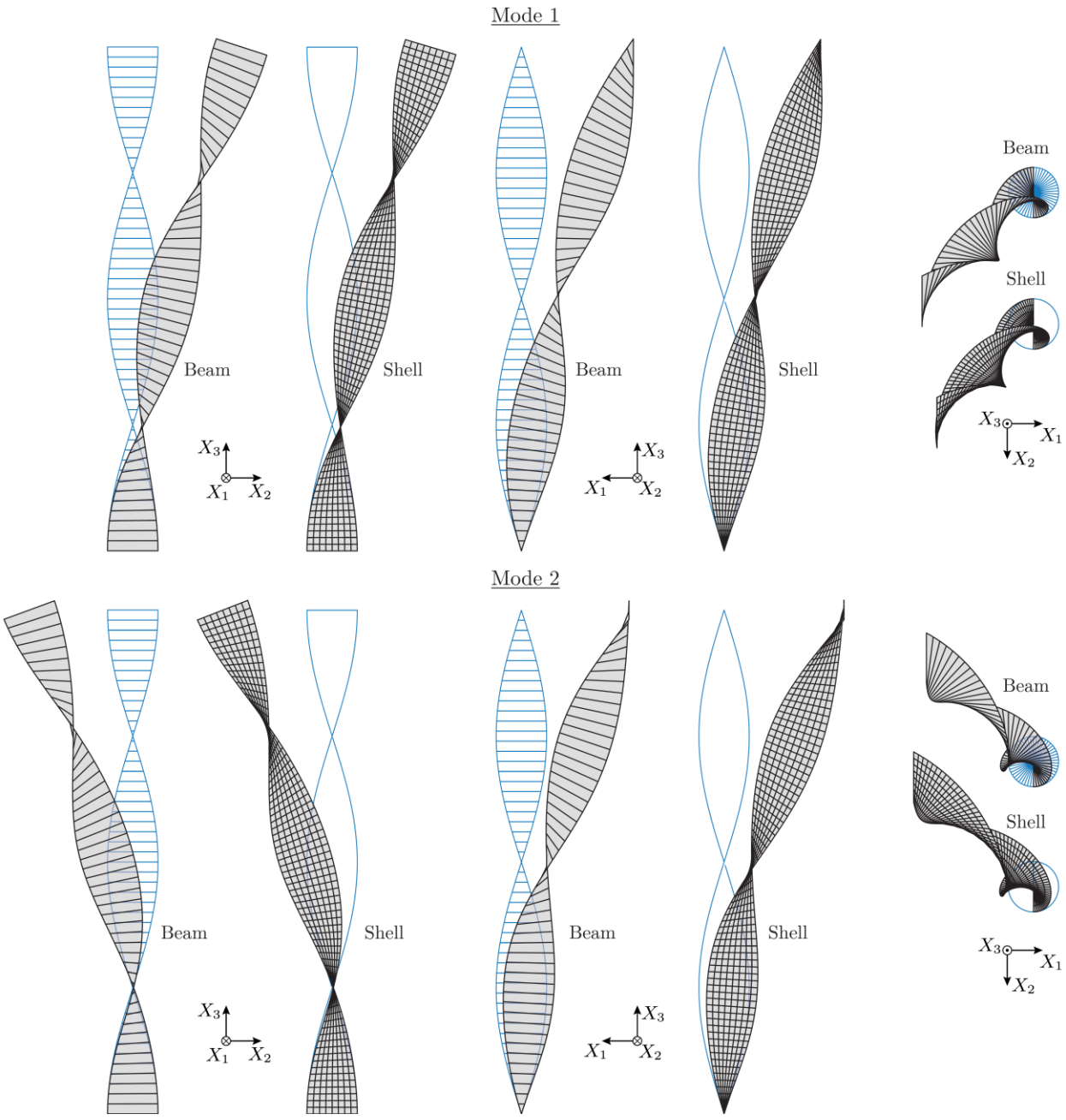

Figure 5: First two buckling modes for a 360º pre-twist

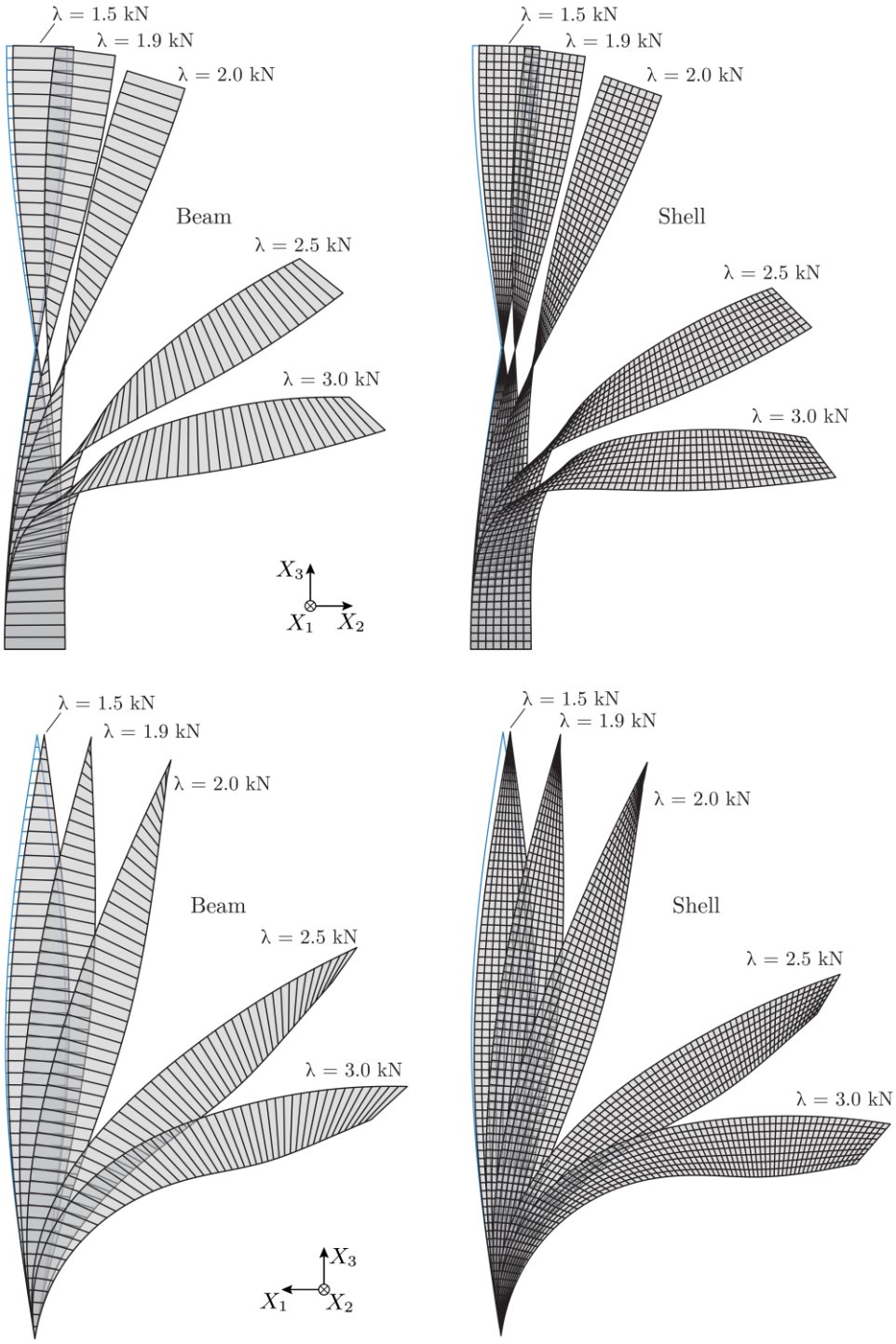

Figure 6: Post-buckling deformed configurations

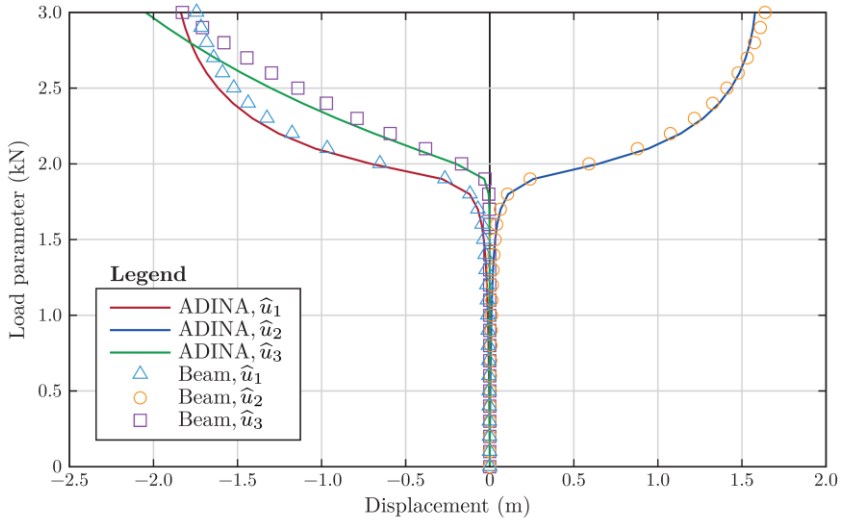

Figure 7: Post-buckling load-displacement paths for a 180º pre-twist

Acknowledgments

This work is part of the research activity carried out at Civil Engineering Research and Innovation for Sustainability (CERIS) and has been funded by Fundação para a Ciência e a Tecnologia (FCT) in the framework of project UIDB/04625/2020.

References

Bathe, K. J. (2022). *ADINA System*, ADINA R&D Inc.

Frisch-Fay, R. (1973). "Buckling of pre-twisted bars." *International Journal of Mechanical Sciences*, 15, 171-181.

Goldstein, H. (1980) *Classical mechanics*, Addison-Wesley.

Gonçalves, R., Ritto-Corrêa M., Camotim D. (2010). "A large displacement and finite rotation thin-walled beam formulation including cross-section deformation", Computer Methods in Applied Mechanics and Engineering, 199(23-24), 1627-1643.

MATLAB (2018), version 9.4.0 (R2018a), The MathWorks Inc., Massachusetts.

Peres N., Gonçalves R., Camotim D. (2021) "A geometrically exact beam finite element for curved thin-walled bars with deformable cross-section." Computer Methods in Applied Mechanics and Engineering, 381, 113804.

Reissner, E. (1972). "On one-dimensional finite-strain beam theory: the plane problem." *Z. Angew. Math. Phys.*, 23(5), 795-804.

Reissner, E. (1973). "On one-dimensional large-displacement finite-strain beam theory." *Studies in Applied Mathematics*, 52, 87-95.

Ritto-Corrêa, M., Camotim, D. (2002). "On the differentiation of the Rodrigues formula and its significance for the vector-like parameterization of Reissner-Simo beam theory." *International Journal for Numerical Methods in Engineering*, 55, 1005-1032.

Rosen, A. (1991). "Structural and dynamic behavior of pretwisted rods and beams." *Applied Mechanics Reviews*, 44(12), 483-515.

Simo, J. (1985) "A finite strain beam formulation. The three-dimensional dynamic problem. Part I." *Computer Methods in Applied Mechanics and Engineering*, 49(1), 55-70.

Steinman, D., Tabarrok, B., Cleghorn, W. (1991). "The effect of pretwisting on the buckling behaviour of slender columns." *International Journal of Mechanical Sciences*, 33(4), 249-262.

Tabarrok, B., Yuexi, X., Steinman, D. (1990). "On buckling of pretwisted columns." *International Journal of Solids and Structures*, 26, 59-72.

Zickel, J. (1956). "Pretwisted beams and columns." *Journal of Applied Mechanics*, 23, 165-175.

Ziegler, H. (1951). Stabilitätsprobleme bei geraden Stäben und Wellen." *Zeitschrift für angewandte Mathematik und Physik*, 2, 265-289.